0254-6124/2026/46(4)-0944-17 *Chin. J. Space Sci.* 空间科学学报

WANG Chi, ESCOUBET Philippe, FORSYTH Colin, DAI Lei, REN Yong, LI Jing, LI Huawang, KONG Linggao, WANG Jindong, WANG Yongmei. Recent Scientific Progress and Mission Update for the Solar Wind Magnetosphere Ionosphere Link Explorer (SMILE). *Chinese Journal of Space Science*, 2026, **46**(4): 944–960. CSTR:32142.14.cjss.2026–yg10. DOI:10.11728/cjss2026.04.2026–yg10

Recent Scientific Progress and Mission Update for the Solar Wind Magnetosphere Ionosphere Link Explorer (SMILE)*

WANG Chi[1] ESCOUBET Philippe[2] FORSYTH Colin[3] DAI Lei[1]
REN Yong[1] LI Jing[1] LI Huawang[4] KONG Linggao[5,1]
WANG Jindong[1] WANG Yongmei[1]

1(*National Space Science Center*, *Chinese Academy of Sciences*, *Beijing* 100190)

2(*European Space Agency/European Space Research and Technology Centre*, *Noordwijk* 2201 *AZ*)

3(*Mullard Space Science Laboratory*, *University College London*, *London RH5 6 NT*)

4(*Innovation Academy for Microsatellites*, *Chinese Academy of Sciences*, *Shanghai* 201304)

5(*Institute of Science and Technology for Deep Space Exploration*, *Suzhou Campus*, *Nanjing University*, *Suzhou* 215163)

Abstract The Solar Wind Magnetosphere Ionosphere Link Explorer (SMILE) mission aims to study solar wind-magnetosphere-ionosphere coupling globally. This review summarizes recent scientific progress and mission status relevant to future SMILE observations. The focus is on dayside magnetopause and cusp dynamics, soft X-ray image interpretation, magnetic-reconnection-driven convection, and storm-substorm coupling. The recent progress of the SMILE platform, payloads, ground segment, and commissioning plan is also briefly reviewed. These studies and mission developments provide the physical and observational basis for interpreting SMILE observations during the early science phase and beyond.

Key words SMILE, Soft X-ray Imager, Ultra-violet Imager, Light Ion Analyzer, Magnetometer, Storm-substorm coupling, Magnetospheric convection, Magnetosheath transients

Classified index P353

1 Introduction

Understanding and predicting the nonlinear, system-level behavior of Earth's magnetosphere remains a grand challenge in solar-terrestrial physics. *In-situ* measurements have greatly advanced our knowledge of localized plasma processes. However, it remains difficult to assemble these local processes into a coherent global picture of magnetospheric dynamics. This difficulty is especially important for the solar wind-magnetosphere-ionosphere system, where the evolution depends on multiscale energy and mass transport and on coupling among different regions. Large-scale structures, including the bow shock, magnetopause, magnetosheath, cusps, and auroral oval, respond continuously to changes in solar wind dynamic pressure and interplanetary mag-

* Supported by the Strategic Priority Research Program on Space Science, the Chinese Academy of Sciences (XDA15350000)

Received May 20, 2026

©The Author(s) 2026. This is an open access article under the CC-BY 4.0 License (https://creativecommons.org/licenses/by/4.0/)

netic field orientation. A key challenge, therefore, is to move from local descriptions of individual plasma processes toward a global and time-dependent view of the geospace system[1,2].

The Solar Wind Magnetosphere Ionosphere Link Explorer (SMILE) mission is designed to close this system-level observational gap. It combines global imaging with *in-situ* measurements. SMILE carries four instruments: the Soft X-ray Imager, the Ultraviolet Imager, the Light Ion Analyzer, and the Magnetometer. These instruments will obtain soft X-ray images of the dayside magnetosheath and cusps, ultraviolet images of the northern auroral oval, and simultaneous *in-situ* measurements of plasma and magnetic fields. The Soft X-ray Imager observes solar wind charge exchange emissions. Their main near-Earth sources are the magnetosheath and cusps. The magnetopause is not observed directly, but can be inferred from intensity structures in the soft X-ray images. In this way, SMILE directly addresses three mission-level questions: the fundamental modes of dayside solar wind-magnetosphere interaction, the substorm cycle, and the origin of coronal-mass-ejection-driven storms and their relationship to substorms[1,2].

Although routine SMILE science images are not yet available, recent simulation and observational studies have already provided important physical context for future SMILE observations. These studies are closely related to the mission's three science questions. They also address key processes in solar wind-magnetosphere-ionosphere coupling. The main topics include dayside boundary dynamics and structure, magnetosheath transients and magnetopause deformation, convection-driven current-system reorganization, and storm-substorm coupling with associated ionospheric and inner-magnetospheric responses. Accordingly, this review focuses on recent scientific progress from 2024 to 2026 in these areas and provides a brief update on the SMILE mission status, including platform and payload development, instrument testing, ground-segment preparation, launch activities, and in-orbit commissioning.

2 Recent Scientific Progress

2.1 Magnetosheath Transients, Soft X-ray Imaging, and Magnetopause Distortion

On the dayside, solar-wind plasma is first processed at the bow shock. It then flows through the magnetosheath and interacts with the magnetopause and cusp regions. This sequence forms a spatially structured and dynamically variable interaction region[3,4]. A key issue for SMILE observations is that SXI records line-of-sight-integrated soft X-ray emission produced by solar wind charge exchange. It does not image the magnetopause surface directly. The observed morphology therefore reflects both the three-dimensional boundary geometry and the soft-X-ray emissivity distribution along the line of sight. Localized brightening, reconstructed boundary displacement, and cusp-related signatures may have several causes. These include magnetosheath high-speed jets and jet-driven bow waves[5], shock-discontinuity-interaction structures and large-scale magnetopause distortion, storm-time density and speed enhancements with magnetospheric compression, and IMF B_y controlled cusp twisting.

Recent simulations of magnetosheath High-Speed Jets (HSJs) provide a physical basis for interpreting localized soft-X-ray enhancements in the magnetosheath. Ouyang *et al.*[5] used two-dimensional hybrid simulations to investigate HSJs and Bow Waves (BWs) downstream of quasi-parallel bow shocks, and compared the hybrid results with Particle-in-Cell (PIC) simulations under similar setups. Their results show that HSJs can compress the downstream magnetosheath/background plasma, produce local density increases and magnetic pileup, and eventually drive bow waves. Using the simulated H^+ flux and a geocoronal hydrogen distribution, they estimated the soft-X-ray intensity from the bow shock to the magnetopause and found that the soft-X-ray flux associated with HSJs and bow waves is more than one order of magnitude higher than that of the surrounding background magnetosheath plasma. This suggests that SMILE/SXI may distinguish signal differences between background magnetosheath plasma and HSJ-related structures, although realistic line-of-sight integration and exposure-time effects require further modeling.

Guo *et al.*[6] extended the discussion from local shock-scale simulations to a three-dimensional global hybrid simulation of SDI-driven magnetosheath jets, magnetopause response, and synthetic soft-X-ray signals. Their results show that Shock-Discontinuity Interactions (SDIs) deform the bow shock and redirect the so-

lar-wind flow with little deceleration, producing ribbon-like jets flanking the core of a Hot Flow Anomaly (HFA) (Figure 1). These jets span the entire dayside magnetosheath and reach ~40 R_E (Earth radius) along the discontinuity. The SDI-driven structures produce large-scale magnetopause distortion, with amplitudes up to ~5 R_E and along-discontinuity extents of ~17 R_E. The study further derived soft-X-ray intensity from a line-of-sight integral of the emissivity and presented synthetic X-ray images. In these images, a pronounced intensity cavity appears at the HFA core, flanked by regions of enhanced X-ray intensity corresponding to the jets. This result links SDI-driven magnetosheath jets, magnetopause distortion, and synthetic soft-X-ray images.

Storm-time magnetopause compression introduces another important limitation for SXI image interpretation. Gong *et al*.[3] simulated dynamic soft-X-ray images generated by SWCX in the Earth's magnetosheath and cusps during the super storm of 10–11 May 2024, using the PPMLR-MHD model and photon-count images derived from SXI simulations. Their analysis evaluated the SXI simulation and the Tangent Fitting Approach (TFA) for reconstructing the 3D structure of the magnetopause under dynamic and non-standard solar wind conditions. The results show that, when the magnetopause is within the FOV, the subsolar magnetopause can be reconstructed with errors within 0.5 R_E. However, under extreme solar wind conditions, the magnetopause location is compressed to 4.9 R_E (Figure 2), which exceeds the FOV of SXI. The limited FOV of SXI and the vignetting effect in SXI imaging therefore need to be considered carefully when interpreting storm-time SXI images and applying boundary tracing methods.

The dayside boundary also includes processes that are not purely magnetosheath transients. Zhang *et al*.[7] reported an O^+-rich ion diffusion region in dayside magnetopause reconnection during the May 2024 superstorm, showing that storm-enhanced ionospheric O^+ can reduce the reconnection rate. Gong *et al*.[6] further showed that the cusp boundary exhibits altitude-dependent three-dimensional twisting controlled by IMF B_y (the y-component of the interplanetary magnetic field), with the twisting angle increasing with both altitude and B_y.

These results support a time-dependent view of the dayside boundary. Because SXI measures line-of-sight-integrated solar wind charge exchange emission, the observed soft X-ray morphology is not a direct map of the magnetopause. It reflects the large-scale geometry of the magnetopause and cusps. It also reflects magnetosheath emissivity variations associated with plasma density and flow structures. Localized enhancements or boundary-

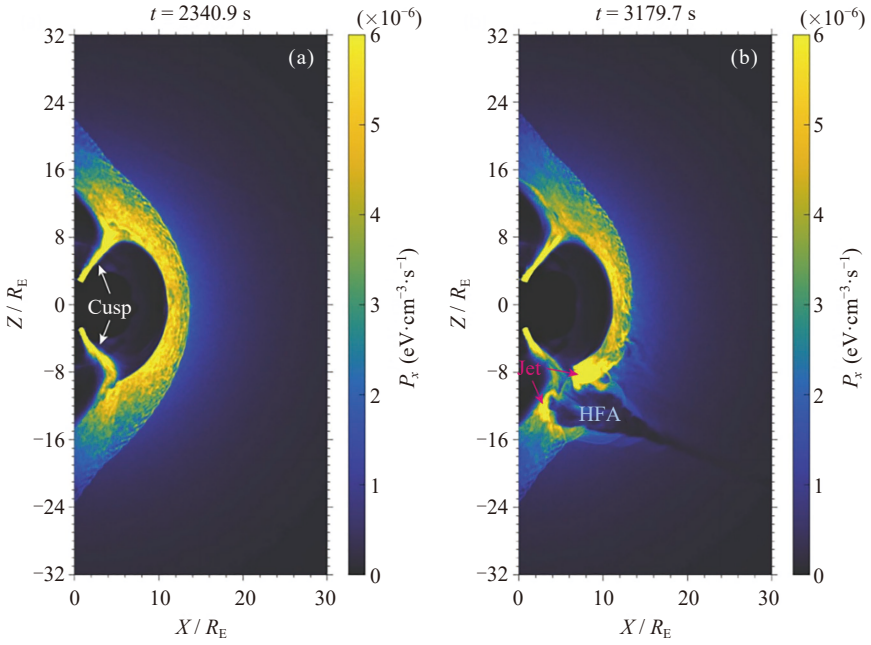


Fig. 1 X-ray image from a lunar-based Soft X-ray Imager based on a three-dimensional global hybrid simulation[4]

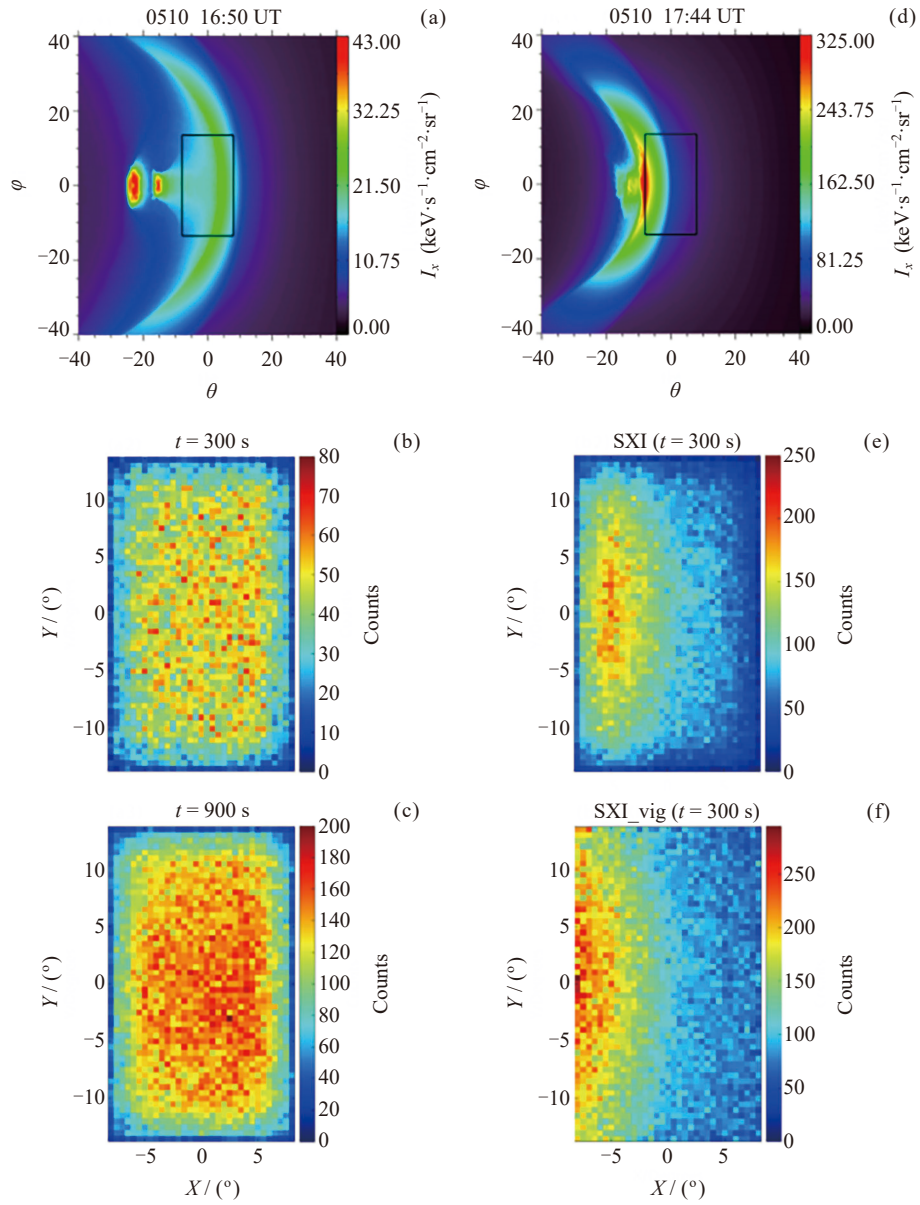


Fig. 2 Soft X-ray images and SXI photon-count images under a special viewing geometry (0510 denotes May 10). Panels (a)–(c) correspond to low solar wind number density: (a) shows the MHD-simulated X-ray image, and (b)–(c) show the SXI photon-count images with exposure times of 300 s and 900 s, respectively. Panels (d)–(f) correspond to high solar wind number density: (d) shows the MHD-simulated X-ray image, (e) shows the SXI photon-count image without the vignetting function, and (f) shows the SXI photon-count image with the vignetting function[3]

like features may therefore have multiple origins. They may trace magnetopause or cusp structures. They may also be influenced by high-speed jets and jet-driven bow waves, shock-discontinuity-interaction-driven jets around a hot flow anomaly core, cusp boundary twisting, storm-time compression, or reconnection-driven erosion of the dayside magnetosphere. The 2024–2026 studies reviewed here provide a physical basis for linking future SXI images to specific dayside boundary processes. They also show that soft X-ray intensity structures should not always be treated as direct boundary traces. UVI auroral imaging provides a complementary diagnostic by indicating whether a dayside disturbance is accompanied by an ionospheric response.

2.2 Reconnection-driven Magnetospheric Convection and Current-system Evolution

Dayside magnetopause reconnection allows solar wind energy and magnetic flux to enter the magnetosphere-ionosphere system[8,9]. Recent studies show that dayside reconnection can directly drive enhanced magnetospheric convection of closed field lines. The convection pattern and associated Region 1 and Region 2 field-aligned currents progress from the dayside to the nightside within about 10–20 min[8-10]. This subsection focuses on how dayside-driven magnetospheric convection is coupled to the evolution of Region 1 and Region 2 field-aligned currents[8,9]. It also discusses its connection to ionospheric two-cell convection and the associated DP-2 current[8,11]. Finally, it considers how large-scale convection electric fields penetrate into the inner magnetosphere[9,12].

Dai *et al*.[8] provide key simulation and observational evidence for this picture (Figure 3). Using global magnetohydrodynamic simulations and magnetosphere-ionosphere observations, they showed direct evidence for dayside-driven magnetospheric convection. An enhanced convection pattern appears within 10 min after the southward turning of the interplanetary magnetic field. The enhanced convection and associated Region 1 and Region 2 field-aligned currents then progress from the dayside toward the nightside within 10–20 min. During this interval, the simulated convection pattern is difficult to attribute to nightside reconnection. The simulations show neither sunward plasma flow nor the associated flow deflection expected from nightside tail reconnection. These results support the idea that dayside reconnection can act as an independent driver of magnetospheric convection. They also link magnetospheric convection to the ionospheric two-cell convection and its associated Hall current (DP-2 current).

The influence of ionospheric conductance on dayside-driven magnetospheric convection has also been quantified in the magnetosphere-ionosphere coupling system. Using global PPMLR-MHD simulations, Zhu *et al*.[9] showed that the temporal and spatial pattern of magnetospheric convection remains largely consistent among the different conductance. However, the convection strength and ionospheric currents change. In the nearly infinite conductance case, the magnetospheric electric field and convection velocity on the equatorial plane decrease by about 20%. In contrast, the ionospheric Region 1 field-aligned current and Pedersen current increase by about 30%. The response time of enhanced magnetospheric convection to the solar wind is not affected by ionospheric conductance. Instead, the 10–20 min timescale may correspond to the anti-sunward drag of reconnected magnetic field lines from the subsolar point to the flank magnetopause. Larger ionospheric conductance makes the ionospheric footprints of dragged field lines more stationary. This leads to stronger Region 1 field-aligned current, larger Pedersen current, and enhanced $\boldsymbol{J} \times \boldsymbol{B}$ force coupling between the ionosphere and magnetosphere, where $\boldsymbol{J}$ is the electric current density and $\boldsymbol{B}$ is the magnetic field.

Solar wind speed provides another important control on dayside-driven magnetospheric convection. Using controlled global MHD simulations with steady upstream parameters, Zhu *et al*.[10] compared fast and slow solar wind streams with speeds of 800 and 400 km·s^{-1}. In the fast-stream case, enhanced convection extends from the dayside magnetopause to 20 R_E downtail within 15 min. This is faster than the approximately 20 min response in the slow-stream case. Fast solar wind also drives stronger and deeper-penetrating convection electric fields in the closed magnetosphere (Figure 4a and 4b). It produces stronger Region 1 field-aligned currents and increased flow shear in the low-latitude boundary layer. The induced convection further shows discrete spatial and temporal channels. Their intervals are about 9 min in the slow-wind case and 2–4 min in the fast-wind case. These results show that solar wind speed controls the timing, penetration depth, and intensity of dayside-reconnection-driven convection.

The same physical chain can extend into the inner magnetosphere. Wang *et al*.[12] analyzed large-scale convection electric fields observed by the Van Allen Probes during 191 isolated high-speed solar-wind-stream events. They found that the convection electric field inside $L < 5.5$ strengthens with both solar wind speed and southward IMF B_z. Its penetration depth also increases with solar wind speed (Figure 4c). When the solar wind speed exceeds about 550 km·s^{-1}, significant convection electric fields can reach L~3. The study further showed that *AU*, *Kp*, and *Dst* respond systematically to convection electric field strength. This result links solar-wind-driven magnetospheric convection to ionospheric elec-

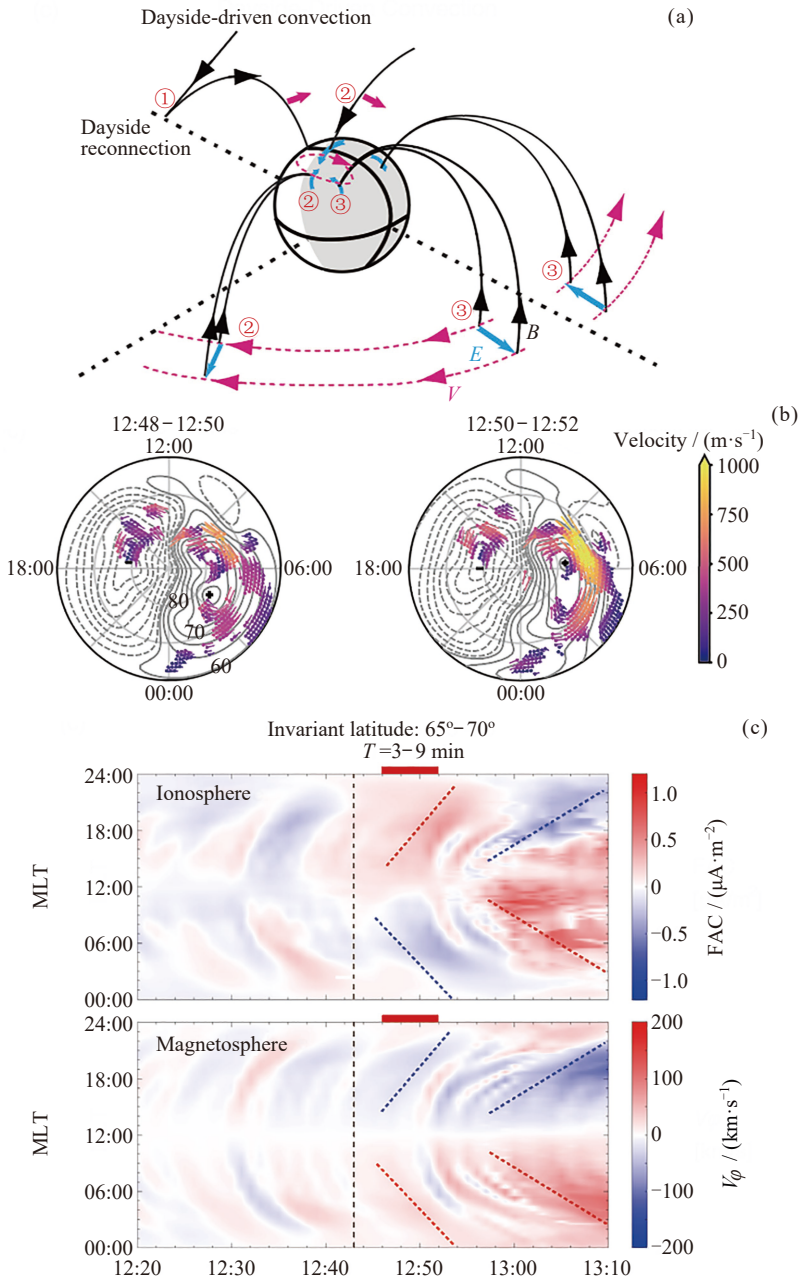


Fig. 3 Dayside-driven magnetospheric convection and its magnetosphere–ionosphere signatures. (a) Schematic of magnetospheric convection driven by dayside reconnection. (b) Ionospheric convection maps. (c) East-West keograms of the Field-Aligned Current (FAC) at the ionosphere and magnetosphere convection, with Local Time (LT) on the horizontal axis[8,14]

trojets, geomagnetic activity, and ring-current development.

Taken together, these studies support a coherent picture of dayside-reconnection-driven magnetosphere-ionosphere coupling. Southward turning of the interplanetary magnetic field initiates or strengthens dayside magnetopause reconnection. This reconnection then drives enhanced magnetospheric convection of closed field lines. The associated convection and Region 1 and Region 2 field-aligned currents progress from the dayside toward the nightside within approximately 10–20 min. Ionospheric conductance affects Region 1 field-aligned current, Pedersen current, current conservation, and the strength of magnetospheric convection. However, it does

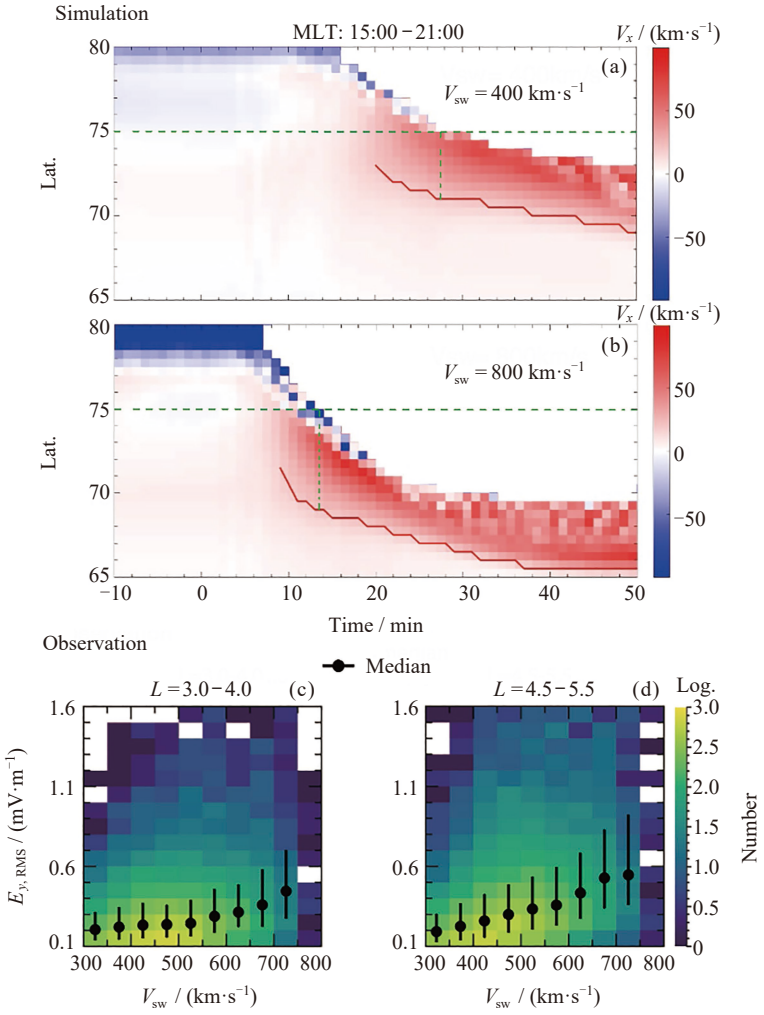


Fig. 4 Solar-wind-speed control of magnetospheric convection and inner-magnetospheric convection electric fields[10,12]

not change the response time of enhanced convection to the solar wind. Solar wind speed further controls the spatiotemporal evolution, penetration depth, intensity, and discrete channels of dayside-reconnection-driven convection. Under high-speed solar wind conditions, large-scale convection electric fields can penetrate deeply into the inner magnetosphere and reach lower L-shells. These studies therefore connect dayside reconnection with global convection and field-aligned-current evolution, DP-1 and DP-2 current-system development, storm-substorm coupling, and inner-magnetospheric convection electric fields.

This subsection suggests a timing and morphology test based on UVI auroral imaging. SXI observations can provide global context for the dayside configuration. UVI is especially relevant because the ionospheric response to magnetospheric convection and field-aligned-current reorganization is expressed through auroral morphology. Time sequences of UVI images can be used to examine auroral oval evolution. Key signatures include dayside auroral responses, magnetic-local-time-dependent auroral expansion, equatorward or poleward displacement, and nightside auroral intensification. These signatures can be compared with simulations, *in-situ* measurements, and ground-based indices. Such comparisons can test whether the ionospheric response evolves on the 10–20 min timescale identified in recent convection studies. Thus, UVI provides an important diagnostic for dayside-driven convection and ionospheric current-system evolution. SXI supplies the corresponding dayside context.

2.3 Storm-substorm Coupling and Ionospheric/ Inner-magnetospheric Responses

Storms and substorms involve a chain of linked process-

es, including changes in solar-wind driving, magnetospheric convection, magnetic reconnection, electric current systems, auroral activity, and energetic particles[12]. Recent studies increasingly emphasize that these processes should be examined through cross-regional coupling within the solar wind-magnetosphere-ionosphere system. The central issue addressed in this subsection is the role of enhanced dayside-driven convection and Region 1 FACs in triggering substorm onset[13]. A second issue is how dominant dayside and nightside reconnection organize the DP-2 and DP-1 components of auroral electrojets[11]. A further issue is how large-scale convection electric fields penetrate into the inner magnetosphere and influence geomagnetic indices, and how storms reshape the energy-dependent radial distribution of outer-belt electron fluxes.

The evolution of magnetospheric convection provides a useful framework for understanding storm-substorm coupling. Within this framework, the convection-driven motion of frozen-in magnetic field lines reorganizes large-scale current systems and governs the development of storms and substorms. This perspective is directly supported by recent work on solar-wind triggering of substorm onset during the May 2024 superstorm. Using coordinated global observations and simulations, REN *et al.*[14] showed that a shock-compressed southward interplanetary magnetic field enhanced dayside-driven convection, Region 1 field-aligned currents, and auroral currents (Figure 5). These disturbances extended rapidly from the dayside toward the nightside, and substorm expansion was initiated within ~6 min. Global simulations further showed that dayside-driven convection of closed field lines depleted nightside flux and thinned the near-Earth current sheet. This process lowered the onset threshold. After onset, nightside flux loading became significant. A reconnection X-line formed near 10 R_E and extended azimuthally. The westward electrojet then connected with Region 1 field-aligned currents to form the substorm current wedge. Together, these studies link magnetospheric convection evolution, current-system development, and the intrinsic relationship between storms and substorms within a single solar wind-magnetosphere-ionosphere coupling picture.

A complementary view comes from recent work on global current-system evolution. Using coordinated observations of storm-time intense substorms, WANG *et al.*[11] showed that substorm expansion is embedded within a global cycle of field-aligned currents and auroral electrojets. This cycle is coupled to large-scale plasma convection. It appears as coherent motion of current peaks across magnetic local time and magnetic latitude. The peaks first move antisunward and equatorward, and then return sunward and poleward. The cycle involves two auroral electrojet components (Figure 6): the convection-driven DP-2 current and the expansion-phase DP-1 substorm current. The antisunward-equatorward phase corresponds to intervals dominated by dayside reconnection. It begins with DP-2 and can transition stepwise into DP-1. The following sunward-poleward phase reflects intervals dominated by nightside reconnection. During this phase, DP-1 may either persist from the preceding interval or develop newly. These observations connect the expanding-contracting polar cap paradigm with the DP-1/DP-2 paradigm. They show that DP-1 onset can occur under either dayside- or nightside-dominated reconnection, whereas the full development of DP-1 commonly involves nightside-dominated reconnection.

Outer-radiation-belt morphology provides a further inner-magnetospheric consequence of storm-time coupling. WANG *et al.*[14] statistically analyzed the peak flux position L_{peak} and inner boundary position L_{min} of the outer radiation belt across storm phases using Van Allen Probes electron flux data from 226 keV to 2.6 MeV. They found an energy-dependent evolution of the outer radiation belt morphology. In the early recovery phase, L_{peak} converges to approximately L = 4.3–4.6 across the analyzed energy range, while L_{min} remains nearly unchanged for electrons above 1 MeV. These results indicate that storm-time convection activities, radial diffusion, local wave acceleration, and loss processes together shape the energy-dependent morphology of the outer radiation belt. Although the outer radiation belt is not a direct SXI or UVI imaging target, its storm-phase evolution represents an important inner-magnetospheric consequence of global solar-wind-magnetosphere driving.

For SMILE interpretation, the key issue is to distinguish convection-driven DP-2 responses from expansion-

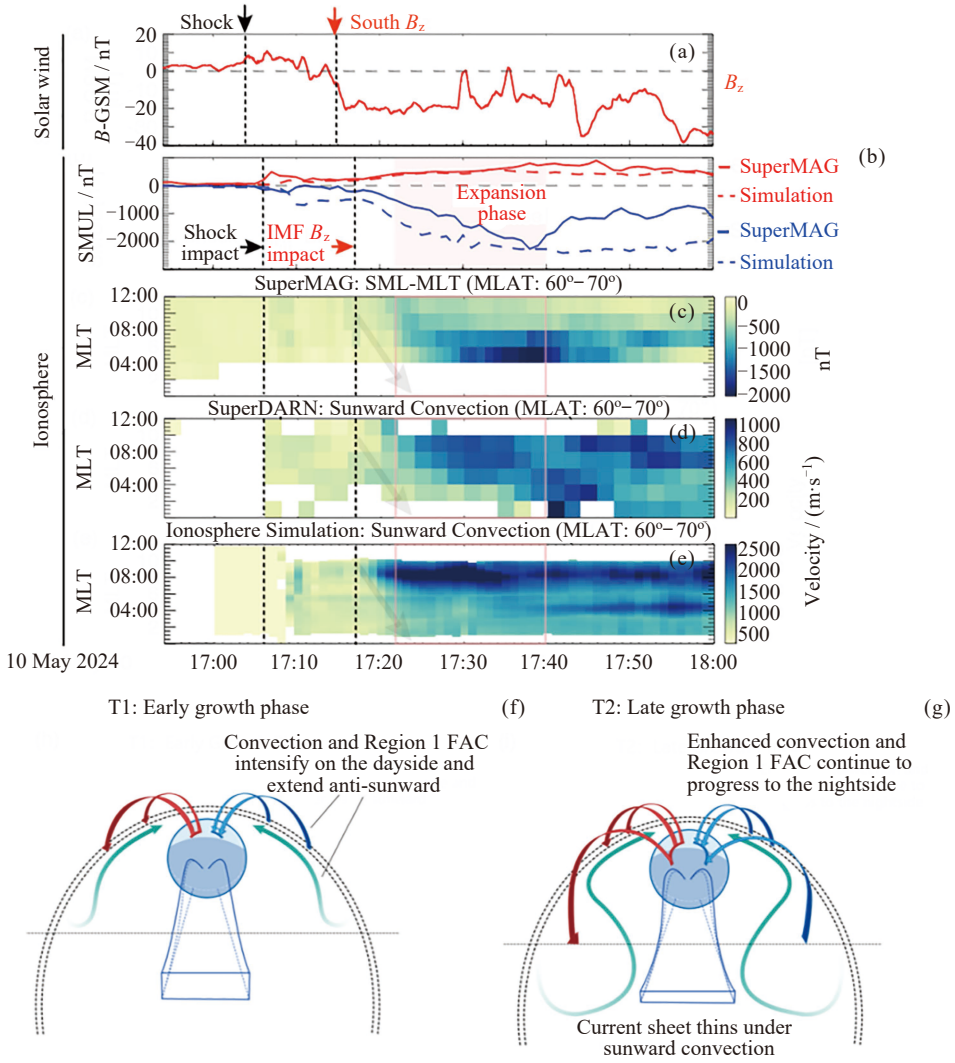


Fig. 5 Solar-wind triggering of substorm onset during the 10 May 2024 superstorm. (a) Magnetic field (the *z*-component of the interplanetary magnetic field, B_z). (b) Auroral electrojet indices. (c) Magnetic-local-time distribution of the SuperMAG auroral Lower (SML) index. (d)–(e) Observed and simulated sunward ionospheric convection, with Local Time (LT) on the horizontal axis. (f)–(g) Schematic illustration of the early and late growth phases, showing the antisunward progression of enhanced convection and Region 1 field-aligned currents and the thinning of the near-Earth current sheet before substorm onset. The vertical axes show the magnetic field in Geocentric Solar Magnetospheric (GSM) coordinates, the SuperMAG auroral Upper and Lower (SMUL) indices, and Magnetic Local Time (MLT), respectively[14]

phase DP-1 and the development of the substorm current wedge. UVI observations, together with ground magnetic indices, SuperDARN convection maps, AMPERE FACs, and simulations, can help determine whether a storm-time substorm sequence is dominated by prompt dayside-driven convection, nightside loading-unloading evolution, or both. SXI provides the simultaneous dayside context through soft-X-ray imaging of the magnetopause, cusps, and magnetosheath structures.

3 Mission Update

3.1 Platform

The PF structure is a stacked structure, including the PM structure comprised of a large Carbon Fiber Reinforced Polymer (CFRP) primary structure and four propellant

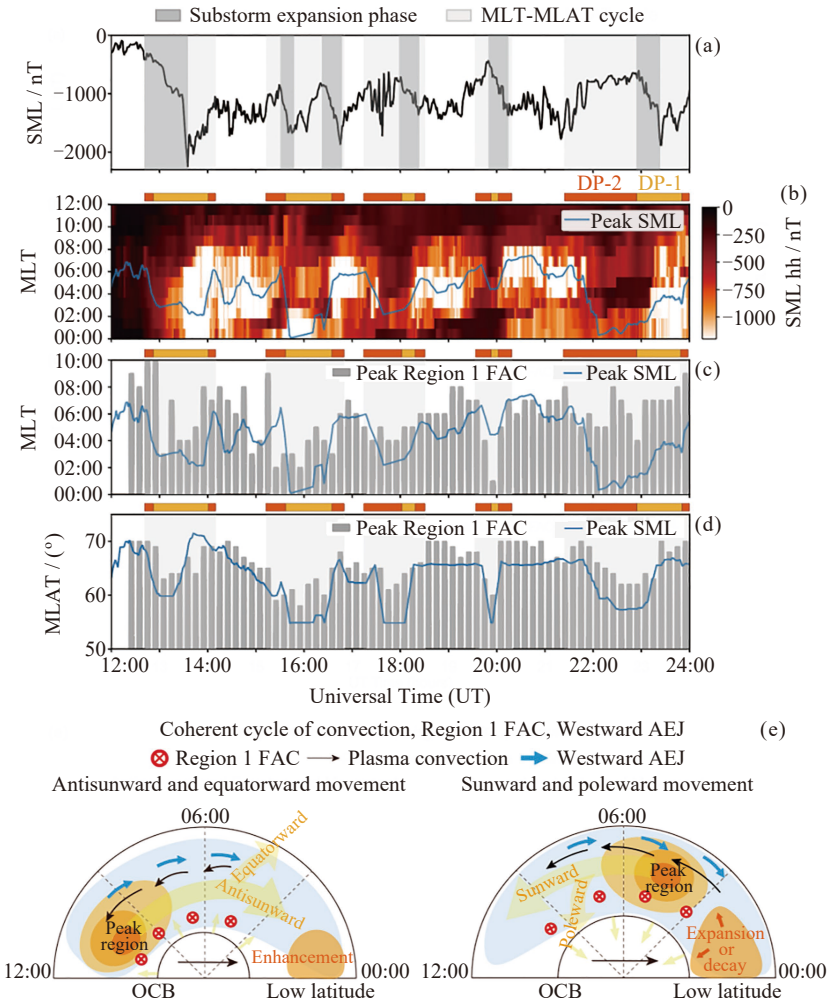


Fig. 6 Global cycle of field-aligned currents and auroral electrojets during storm-time substorms. (a) SML index. (b) Magnetic-local-time distribution of the westward auroral electrojet. (c)–(d) Temporal evolution of the magnetic local time and magnetic latitude of the peak Region 1 field-aligned current and peak SML. (e) Schematic illustration of the coherent cycle of plasma convection[11]

tanks, and the cubical-shaped SVM structure featuring several honeycomb panels and CFRP frames. There are two solar arrays mounted on the SVM $+Y$ and $-Y$ lateral panels, which are installed and deployed by two solar array mechanisms. The assembly of SVM and PM flight models has been completed in April 2024. And finished the environment tests during May to August 2024 (Figure 7–9).

3.2 Payload Module (PLM)

UVI FM is the latest instrument that delivered to PLM in December 2024. Then PLM FM finished the final integration and delivered to ESTEC. The UVI FM and PLM FM already completed the environment test separately and will join in the SC level environment test for the next step.

3.3 Instruments

3.3.1 SXI

SXI will use novel soft X-ray imaging technology to obtain global images of the large-scale structures of the magnetosheath for the first time. This is critical to understand the key features of magnetospheric global dynamics. SXI consists of a main telescope, an SXI electronics box and the front-end electronics. The telescope uses a Lobster-eye technique based on micropore optics to focus the X-rays onto the two very large CCD arrays located on the focal plane. The focal plane is protected from potential radiation damage by a shutter mechanism. Figure 10 shows the SXI Telescope Flight Model (FM) during integration in laboratory. SXI FM delivered to PLM in June 2024.



Fig. 7 Platform thermal vacuum test in May 2024



Fig. 8 Platform mechanical test in June 2024

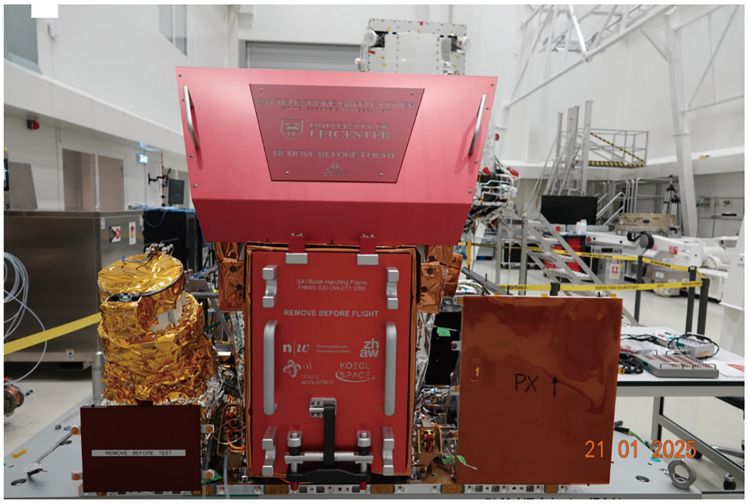


Fig. 9 PLM inspection before delivery in ESTEC in January 2025

3.3.2 UVI

UVI will capture global images of the aurora borealis with high spatial resolution. UVI consists of two key sub-assemblies: the optical module (UVI Camera, UVI-C), which is the heart of the instrument; and the electrical control unit (UVI-E). Due to the responsibilities for the development of UVI change to CAS with contributions from ESA. This caused a delay in the development of UVI. However, CAS and ESA are doing their utmost to minimize the schedule impact. The UVI-C Qualification Model (QM) has completed delivery to Airbus in May 2024, and completed the integrating test and environment test with PLM/FM. Following the development of QM, the UVI/FM completed the unit function test, qualification test and final calibration test. In October 2024, UVI FM passed the QAR and PSR organized by CAS and ESA. UVI FM delivered to ESTEC and integrated with PLM in November 2024. UVI FM takes part in all tests with the spacecraft and pre-launch activities in 2025, including deployment test. The FM of UVI is shown in Figure 11.

3.3.3 MAG

The MAG instrument will measure the *in-situ* magnetic field using a digital fluxgate magnetometer system consisting of two individual tri-axial fluxgate sensor heads mounted on a 3-meter-long deployable boom. In March 2024, MAG FM passed the QAR and PSR organized by CAS and ESA. It has now been delivered to Airbus, which is the first instrument of SMILE that has been delivered to ESA. The FM of MAG boom and electronic box are shown in Figure 12.

After delivery, the MAG instrument was mounted to PLM and finished integration tests. In Nov. 2024, after PLM level deployment test, the MAG was integrated to SMILE spacecraft in ESTEC together with the PLM. In 2025, the MAG instrument finished spacecraft level mechanical, thermal and EMC test. The spacecraft level MAG Boom deployment test was finished in July 2025, supported by 3 Helium blooms, the boom was deployed successfully. The deployment test scene is shown in Figure 13.

3.3.4 LIA

Two identical LIA sensors are designed on the basis of a top-cap electrostatic analyzer for large dynamic flux range, wide Field of View (FOV) and high-resolution ion measurement. Since each LIA has 2π FOV, a large 4π FOV for the ion measurement can be achieved overall by the two LIAs. The FM of one LIA instrument is shown in Figure 14. The FMs of LIA have been calibrated at the National Space Science Center (NSSC) and

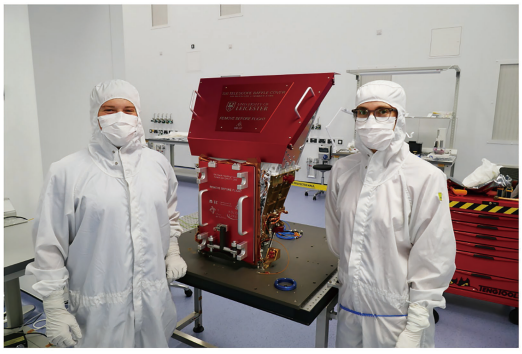


Fig. 10 SXI Telescope FM in laboratory (credit to Leicester U., UK)

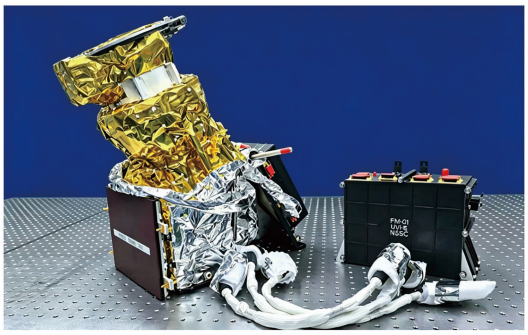


Fig. 11 UVI FM

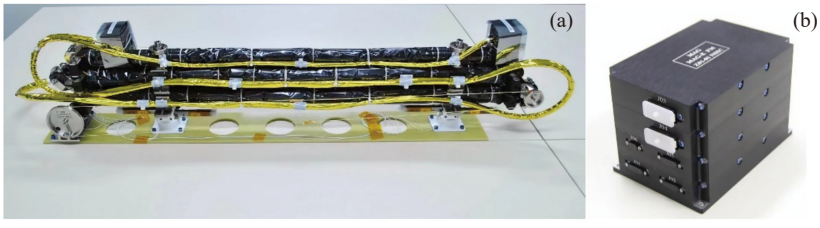


Fig. 12 FM of MAG boom (a) and electronic box (b)



Fig. 13 MAG boom deployment test in July 2025 in ESTEC

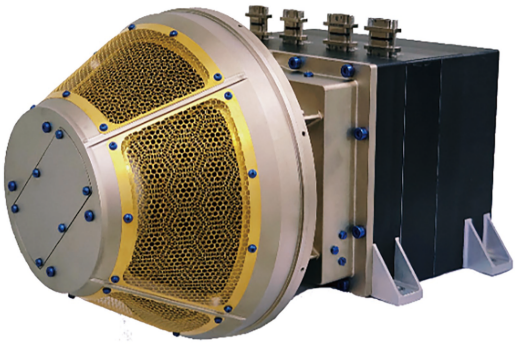


Fig. 14 FM of LIA

cross calibration has been carried out in the Mullard Space Science Laboratory (MSSL) in September 2024. The calibration results at NSSC and MSSL are consistent very well. LIA has completed its QAR and delivered the FMs to ESTEC for spacecraft level tests in October 2024. LIA FMs were sent back to NSSC for performance check after all the tests done at ESTEC in September 2025. No performance degradation has been found after the performance check. The LIA FMs have been sent back to ESTEC in November, 2025 for the further integration and launch activities.

3.4 Ground Segment

The Ground Segment (GS) of the SMILE mission is jointly established by CAS and ESA. The GS architecture is illustrated in Figure 15 to demonstrate the respective responsibilities and ground-to-space links. The ground segment responsibilities and operation principles for CAS are science operations (joint responsibility), mission operations, telemetry, S-band Tracking and Command (TT&C) ground stations, X-band payload data communication station (Sanya as backup). The ground segment responsibilities and operation principles for ESA are Science Operations (joint responsibility), S-band TT&C ground stations (as support to Mission Operations), X-band payload data communication stations (DLR station as baseline).

The network link between ESOC and CCC is critical during launch and SC orbit transfer activities. So the backup link are established and tested before launch under CAS's responsibilities. The Ground segment operation rehearsal are completed in 2025 and the interface between units are compatible and verified.

3.5 Launch Vehicle

SMILE will be launched by a Vega-C VV-29 rocket provided by AVIO. The fit check with the satellite and the launch vehicle adapter has been conducted at the beginning of 2023 and did the fit check again for the FM in September 2025 in ESTEC as Figure 16.

Platform (PF) FM completed all environmental tests in IAMC before September 2024 and then prepare the shipment to ESTEC especially for the export control and also dangerous goods process. PF FM arrived ESTEC in December 2024 after the effort by CAS and ESA. After the successful interface test between PF and PLM, then start the SC integration and completed at the end of January 2025 as Figure 17.

SMILE SC completed EMC, AC magnetics, sine vibration, acoustics, solar panel deployment, thermal

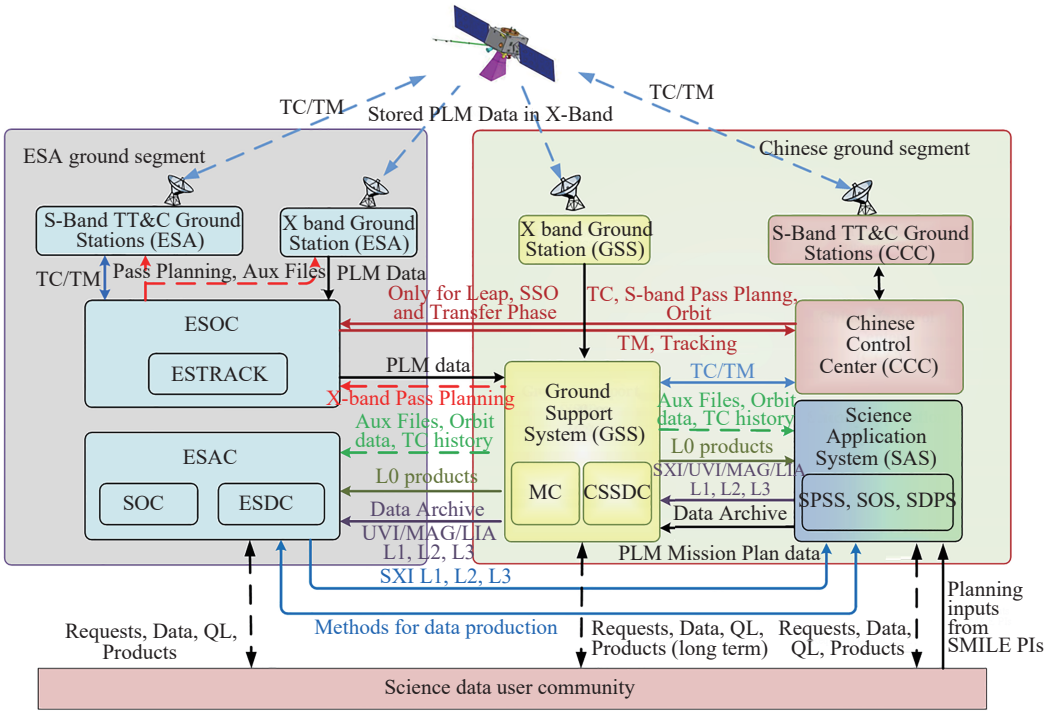


Fig. 15 SMILE ground segment architecture



Fig. 16 Vega-C fit Check with FM S/C in September 2025 in ESTEC (Credit to ESA/CAS)

vacuum, DC magnetics tests and fit check with launcher from February to September 2025. After the final settlement of MLI and cleanliness of SC and then keep the SC in the container and waiting for the transportation from ESTEC to French Guyana Space Center.

SMILE SC and Ground Support Equipment (GSE) start the transportation in the beginning of February of 2026 from Amsterdam harbor to Kourou by boat through Atlantic Ocean (Figure 18). SMILE and GSE arrived Kourou two weeks later and transferred to S3 B clean-room in CSG (Centre Spatial Guyanais). Then start SC inspection, alignment, functional and leakage test after the transportation. The SC was filled with propellant in March and delivered to AVIO to make installation with Vamper 1194 and capsuled in the Fairing (Figure 19). The SMILE satellite was launched on 19 May 2026 by Vega-C VV29 very smoothly as textbook. Now the satellite status is stable and already start the transfer obit



Fig. 17 SC integration in January 2025 in ESTEC (Credit to ESA/CAS)



Fig. 18 SC transportation in Amsterdam harbour

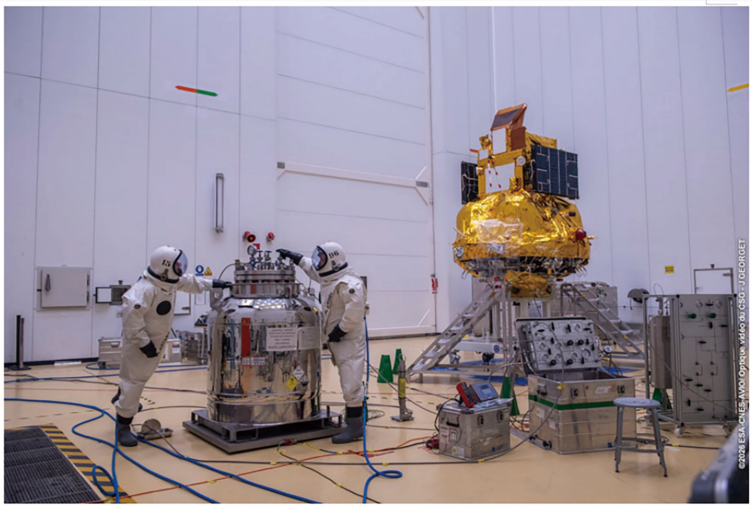


Fig. 19 SC was filled in propellant in S3 B

for the second time. The SMILE satellite will reach the scientific orbit before end of June and then start the operation of instruments and in orbit commissioning. The IOCR (In Orbit Commission Review) will be held before end of September 2026 and then hand it over for GSS to operate and science team start to use the data for scientific analysis.

3.6 Post-launch Milestones

SMILE was successfully launched aboard a Vega-C rocket on flight VV29 on 19 May 2026. After launch, the spacecraft entered the orbit transfer phase. From 19 May to the end of June 2026, the satellite is planned to transfer from its initial 700 km circular orbit to the highly elliptical science orbit, with an altitude range of approximately 5000–121000 km. From early July to early September 2026, spacecraft and payload in-orbit commissioning tests will be carried out. The CAS-ESA joint In-Orbit Commissioning Review (IOCR) is expected to be completed in mid-September 2026, after which the mission will be handed over for science operations. According to the current mission plan, SMILE is designed for a nominal three-year in-orbit operation. A possible mission extension will be considered according to the spacecraft status and scientific operation needs.

4 Summary and Outlook

The studies reviewed here support a system-level perspective on solar wind-magnetosphere-ionosphere coupling. The main processes should not be treated as isolated elements. Dayside boundary dynamics, reconnection-driven convection, current-system evolution, auroral activity, and inner-magnetospheric responses form a connected geospace chain. On the dayside, SXI-relevant soft-X-ray morphology is controlled by both boundary geometry and magnetosheath emissivity. The relevant geometry includes the magnetopause and cusps. The emissivity depends on plasma density and flow structures in the magnetosheath, and can be modified by high-speed jets, jet-driven bow waves, shock-discontinuity-interaction jets, HFA-related cavities, storm-time compression, and IMF B_y-dependent cusp twisting. In the magnetosphere-ionosphere system, dayside magnetic reconnection can rapidly drive closed-field-line convection within about 10–20 min after southward IMF turning. Region 1 and Region 2 field-aligned currents evolve with this convection. Ionospheric conductance affects current closure and convection strength, while solar wind speed controls the timing, intensity, penetration depth, and channelized structure of the response. During storms and substorms, this convection-centered picture links dayside triggering with nightside loading–unloading evolution. It also links DP-2 and DP-1 auroral-electrojet development, formation of the substorm current wedge, inner-magnetospheric convection electric fields, and radiation-belt responses.

This system-level picture also defines the observational role of SMILE. SXI provides global soft-X-ray context for the dayside magnetosheath, magnetopause, and cusps. UVI records the corresponding auroral and current-system responses in the ionosphere. These two image products therefore represent different parts of the same solar wind-magnetosphere-ionosphere coupling chain. Ground-based observations and numerical simulations are needed to connect dayside forcing, global boundary motion, ionospheric convection, and auroral current-system evolution. Within this framework, time sequences of UVI images can be used to assess how dayside solar-wind forcing is transmitted to auroral morphology changes, convection-driven FAC/electrojet reorganization, and expansion-phase substorm current-system development.

This connection becomes especially important as SMILE enters the stage of early observations and data interpretation. The scientific studies reviewed here are therefore not only preparatory studies for a future imaging mission. They also provide a practical basis for interpreting early SMILE observations once the mission begins science operations. In this sense, recent scientific progress and mission progress are closely linked. The mission update shows that SMILE is approaching the stage in which global SXI and UVI image sequences can be used to test the physical scenarios developed in recent simulations and coordinated observations.

Future SMILE-era studies will need to clarify how the 10–20 min directly driven dayside-convection response is related to the classical ～1 h loading-unloading response during storms and substorms. This issue is particularly important when convection-driven DP-2 signatures and expansion-phase DP-1 signatures coexist in

auroral electrojets and field-aligned current systems. Synthetic SXI/UVI observations, multi-instrument timing analysis, ground-based observations, and model-data comparisons will be useful for connecting dayside forcing with ionospheric and inner-magnetospheric responses. With SMILE observations, these approaches may help convert global soft-X-ray and ultraviolet image sequences into a quantitative understanding of solar wind-magnetosphere-ionosphere coupling.

Conflict of Interests The authors declare that there is no conflict of interests

References

[1] WANG C, BRANDUARDI-RAYMONT G. Update on the ESA-CAS joint Solar wind Magnetosphere Ionosphere Link Explorer (SMILE) mission[J]. *Chinese Journal of Space Science*, 2020, **40**(5): 700-703

[2] WANG C, ESCOUBET P, FORSYTH C, *et al*. Recent progress of the Solar wind Magnetosphere Ionosphere Link Explorer (SMILE) mission[J]. *Chinese Journal of Space Science*, 2024, **44**(4): 692-698

[3] GONG Y Q, SUN T R, TANG B B, *et al*. Dynamic X-ray imaging of the magnetosheath expected during a super storm[J]. *Frontiers in Astronomy and Space Sciences*, 2025, **12**: 1563653

[4] GUO J, LU S, LU Q M, *et al*. Large-scale magnetosheath jets formed by shock-discontinuity interactions: a three-dimensional global hybrid simulation[J]. *Geophysical Research Letters*, 2026, **53**(9): e2025GL121533

[5] OUYANG W X, YANG Z W, GUO X C, *et al*. Magnetosheath jet-driven bow waves and their soft X-ray imaging: Hybrid and PIC simulations[J]. *Chinese Journal of Space Science*, 2024, **44**(6): 979-987

[6] GONG Y Q, SUN T R, ESCOUBET C P, *et al*. The effects of IMF B_y on the twisting of cusp[J]. *Journal of Geophysical Research: Space Physics*, 2026, **131**(5): e2025JA034856

[7] ZHANG A X, DUAN S P, DAI L, *et al*. Observations of the magnetopause reconnection ion diffusion region with high-density O^+ ions during the May 2024 superstorm[J]. *Geophysical Research Letters*, 2026, **53**(8): e2025GL121449

[8] DAI L, ZHU M H, REN Y, *et al*. Global-scale magnetosphere convection driven by dayside magnetic reconnection[J]. *Nature Communications*, 2024, **15**(1): 639

[9] ZHU M H, DAI L, WANG C, *et al*. The influence of ionospheric conductance on magnetospheric convection during the southward IMF[J]. *Journal of Geophysical Research: Space Physics*, 2024, **129**(9): e2024JA032607

[10] ZHU M H, DAI L, REN Y, *et al*. Response of magnetospheric convection to the southward turning of the IMF in fast and slow solar wind streams[J]. *Journal of Geophysical Research: Space Physics*, 2025, **130**(11): e2025JA034529

[11] WANG T H, DAI L, ESCOUBET C P, *et al*. Substorm expansion embedded in a global cycle of field-aligned currents and auroral electrojets[J]. *Nature Communications*, 2026, **17**(1): 2970

[12] DAI Lei, WANG Chi, REN Yong, *et al*. Geomagnetic storms and substorms: progress and perspectives[J]. *Chinese Science Bulletin*, 2025, **70**(27): 4759-4774 (戴磊, 王赤, 任勇, 等. 磁暴和亚暴研究进展与展望 [J]. 科学通报, 2025, **70**(27): 4759-4774)

[13] REN Y, ZHU M H, DAI L, *et al*. Solar-wind triggering of substorm onset during the May 2024 superstorm: coordinated global observations and simulations[J]. *Geophysical Research Letters*, 2026, **53**(4): e2025GL119629

[14] WANG X, DAI L, REN Y, *et al*. The evolution of Earth's outer radiation belt over geomagnetic storm phase in Van Allen Probe era[J]. *Journal of Geophysical Research: Space Physics*, 2024, **129**(11): e2024JA032674

Author Biography



WANG Chi The Director of the National Space Science Center, Chinese Academy of Sciences (CAS), and an Academician of CAS and the International Academy of Astronautics. He received his bachelor's degree from the University of Science and Technology of China in 1990 and his Ph.D. from the Massachusetts Institute of Technology in 1998. His research focuses on space physics and space weather. He currently serves as Chief Scientist of Phase IV of China's Lunar Exploration Program, the Chinese Principal Investigator of the Solar Wind Magnetosphere Ionosphere Link Explorer (SMILE) mission, and Commander-in-Chief of Phase II of the Chinese Meridian Project. His honors include the Special Prize of the National Science and Technology Progress Award, the Qian Xuesen Outstanding Contribution Award, and the First Prize of the Science and Technology Progress Award of the Chinese Geoscience Union.
E-mail: cw@spaceweather.ac.cn